Behaviour of Solid Oxide Fuel Cell Materials in Technological Environments

Viktoriya Podhurska[a*], Bogdan Vasyliv[a], Andrij Ivasyshyn[a], Orest Ostash[a], Oleksandr Vasylyev[b], Tetyana Prikhna[c], Volodymyr Sverdun[c], Yehor Brodnikovskyi[b]

[a] *H.Karpenko Physico-Mechanical Institute, 5 Naukova Street, Lviv 79060, Ukraine*

[b] *I.Frantsevich Institute for Problems in Materials Science, 3 Krzhizhanovsky Street, Kyiv 03680, Ukraine*

[c] *V.Bakul Institute for Superhard Materials, 2 Avtozavodska Street, Kyiv 04074, Ukraine*

podhurskavika@gmail.com

Keywords: *solid oxide fuel cell (SOFC), YSZ–NiO anode ceramics, MAX-phase interconnect, reducing and oxidizing gas environments, physical and mechanical properties, structure.*

The YSZ–NiO ceramics for SOFC anodes and MAX-phases of Ti-Al-C systems for interconnects have been investigated. Based on the tests of YSZ–NiO specimens preconditioned by one-time reduction or by redox cycling at 600 or 800 °C, a certain mode of the material treatment was established which provides its improved physicomechanical properties. The oxidation behaviour of MAX-phases has been investigated at 600 °C in air. It was found that the intense initial oxidation of hot-pressed Ti_3AlC_2-based material can be eliminated by a certain mode of pre-oxidation. The oxidation resistance of the material can be significantly improved by niobium addition.

Introduction

A number of publications predict a dual influence of operating temperature on resulting physical and mechanical properties of the Ni-containing anode material for solid oxide fuel cells (SOFCs) after cyclic reduction–oxidation (redox) treatment [1–3]. It is well known that the electrical conductivity of metallic Ni (of about $1.4 \cdot 10^7$ S/m) is much higher than that of YSZ–Ni cermet. According to our data, after exposition of the ceramics sintered of NiO powder, for 4 h or more in pure hydrogen at 600 °C, complete reduction can be achieved [4]. The resulting electrical conductivity of the material is about $(1–5) \cdot 10^6$ S/m. However, exposition of NiO ceramics at this regime in the Ar–5 vol% H_2 mixture that can be used for gradual reduction of SOFC anodes causes partial reduction of the NiO particles forming thin edgings of metallic Ni (of thickness of 0.1–0.3 μm) around them. Thus, the electrical conductivity of the material treated is in the range of $(1–5) \cdot 10^5$ S/m depending on average particle size, porosity and resulting contacts between Ni edgings. During redox treatment of NiO ceramics, structural transformation of

boundaries of contacting nickel phase particles occurs, causing an increase in strength.

In our previous works, it was revealed for ScCeSZ–NiO anode ceramics that at selected redox treatment regimes when the material is heated in vacuum and intermediate degassing between reduction and oxidation stages is performed, substantial improvements in strength (up to 112 %) and electrical conductivity can be reached at the treatment temperature of 600 °C [5, 6].

Recently, a new classes of materials based on layered carbide Ti_3AlC_2 have attracted a great attention of material scientists due to their exceptional properties. This carbide belongs to so called MAX-phases which have a chemical formula: $M_{n+1}AX_n$ – where M is an early transition metal, A is an A-group element, and X is carbon and/or nitrogen. These materials have good thermal and electrical conductivity, low density, high strength and Young's modulus, excellent thermal shock resistance, high chemical resistance, relatively low thermal expansion coefficient and good machinability [7-9]. Owing to such combination of properties they have been suggested for various application, especially as high-temperature structural materials. This requires comprehensive investigations of oxidation resistance of Ti_3AlC_2 based materials.

In spite of thorough research of oxidation behavior of Ti_3AlC_2 based materials at high temperature [10-13], only a few results obtained at intermediate temperatures have been reported [14, 15]. Take into account the anomalously intense oxidation of Ti_3AlC_2 based material at 500 °C and specially at 600 °C [14] the investigation of oxidation behavior of these materials at intermediate temperatures have a great importance.

The aims of this work are to study the physical and mechanical behaviour of the SOFC anode and interconnect material and to find out the microstructural changes causing resulting properties of the material.

Experimental part

Materials

Anode ceramics of the YSZ–NiO system sintered at Forschungszentrum Jülich (Germany) of zirconium oxide powder stabilized with 8 mol% Y_2O_3, with the addition of 50 wt% NiO, has been investigated.

The interconnect materials used in this work were initially sintered in vacuum from mixture of TiC, TiH_2 and Al powders and then hot pressed at 1350 °C under pressure of 30 MPa for 1 h. The phase composition of sintered material consisted of 95 wt. % Ti_3AlC_2 and 5 wt. % TiC. Fig. 1a shows the back-scattered electron image of polished surface of this material. The equi-axed grains of Ti_3AlC_2, fine particles of TiC and big pores were observed. The porosity of the material determined by the hydrostatic-weighing method was 22%. After hot pressing refinement of the

structure and reducing of the porosity to 1 % have been occurred (Fig. 1b). The amount of Ti_3AlC_2 was decreased to 92 wt. % and TiC increased to 6 wt. %. Additionally, in this material we revealed the 2 wt. % Al_2O_3. The material doped with 3.5 wt. % Nb fabricated by the same process as previous material consisted of 56 wt. % $(Ti, Nb)_3AlC_2$, 41 wt. % TiC and 3 wt. % Al_2O_3. The structure of this material includes equi-axed grains of Ti_3AlC_2 and TiC and uniformly distributed fine particles of Al_2O_3 and small pores (Fig. 1c).

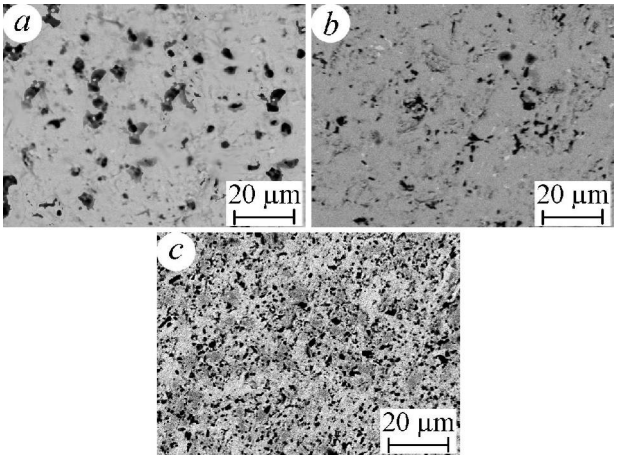

Figure 1. Back-scattered electron images of the polished surfaces: (a) Ti_3AlC_2 based material with 22 % porosity; (b) Ti_3AlC_2 based material with 1 % porosity and (c) Nb dopped Ti_3AlC_2 based material with 1 % porosity.

Methods

A series of YSZ–NiO ceramic specimens of the size of 1×5×25 mm were singly reduced at 600 or 800 °C in a hydrogenous environment (the Ar–5 vol% H_2 mixture or hydrogen of 99.99 vol% H_2 purity) under the pressure of 0.15 MPa (Fig. 2a) or subjected to redox cycling (see Table 1) [16].

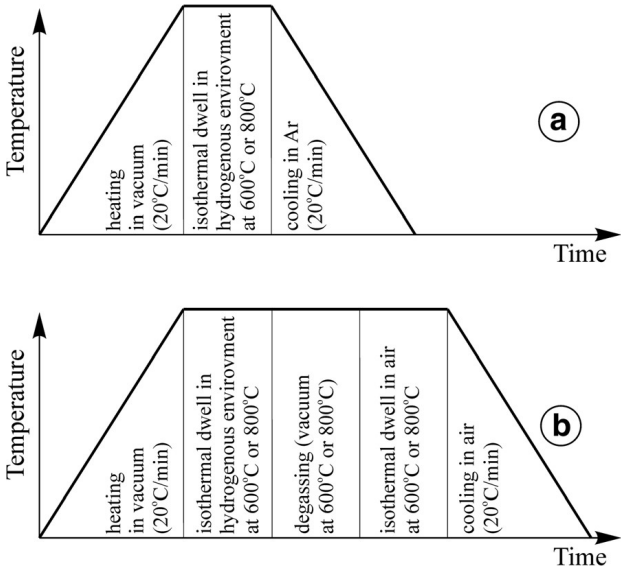

Figure 2. The treatment schemes applied for YSZ–NiO ceramics. a Single reduction in a hydrogenous environment. b A cycle of redox treatment.

The redox treatment of ceramics was performed for five cycles according to the scheme [4]: heating in vacuum from 20 to 600 °C, reduction in a hydrogenous environment at 600 or 800 °C under the pressure of 0.15 MPa, degassing, oxidation in air at 600 °C and cooling down to 20 °C in air (Fig. 2b). Reduction/oxidation stage duration was chosen, taking into account the literature data on complete or partial reduction of the material [17]. After the redox cycling, reduction of materials in a hydrogenous environment for 4 h at 600 °C or for 1 h at 800 °C under the pressure of 0.15 MPa with cooling in argon was performed (see the scheme in Fig. 2a) [16]. The heating/cooling rate was 20 °C/min.

Table 1. The treatment regimes for the materials tested

No. of version	Environment	Treatment temperature (°C)	Reduction/ oxidation stage duration (h)	Variant of treatment
1	Ar–H_2 mixture	600	4	R
2	H_2	600	4	R
3	Ar–H_2 mixture / air	600	4	RO
4	H_2 / air	600	4	RO
5	Ar–H_2 mixture	800	1	R
6	Ar–H_2 mixture / air	800	1	RO

R single reduction, RO redox cycling

The isothermal oxidation tests of interconnect materials were carried out at the temperature of 600 °C in static air using rectangular bars with dimensions of 20×5×3 mm. The specimens were cut by the electrical discharge method, abraded to 1000 grit with SiC paper and polished by diamond past. The oxidation tests were divided into five stages which had the duration: first stage – 15 h, second stage –245 h and the last three stages – 250 h. The each stage consisted of heating to 600 °C in air, exposition for determinated time and cooling to room temperature. The weight of the specimens was measured before the test and after the each stage by analytical balance. The accuracy of the weight measuring was $\pm 10^{-4}$ g. The oxidation resistance of materials tested was characterized by weight gain per unit surface area $\Delta W/S$.

Ultimate fracture stresses of materials in the initial state (σ_{f0}) and after the corresponding treatment (σ_f) were determined during the three-point bending test of the specimens in air at 20°C. Based on these data, the relative strength (σ_f / σ_{f0}) of the material treated was evaluated.

The specific electrical conductivity of the material (σ) was determined in air at 20°C using the Van der Pauw method. SEM microstructures, microfractographs and quantitative elemental content of the specimens were investigated using the electron microscope Carl Zeiss EVO-40XVP coupled with energy dispersive spectroscopy (EDS) INCA ENERGY 350.

The X-ray analysis was carried out using DRON-4.0 diffractometer (Fe K_α) with Bragg-Brentano-type geometry. The total range of angles was from 20 to 120 degrees. The step was 0.05 degree and total test duration was 8 hours.

The average size of coherent dispersion areas of nickel phase (D) was calculated using the Win CSD program [18]. The spacing between the planes in the atomic lattice (d) of zirconia phase (line 220) was estimated using the Rietveld method [18], and the residual stresses (σ_r) were evaluated using the equation

$$\sigma_r = -\frac{E}{\nu} \cdot \frac{d - d_0}{d_0} \qquad (1)$$

where E is Young's modulus and ν is Poisson's ratio; the values of these parameters were selected according to [19]; d_0 is the spacing between the planes in the atomic lattice of zirconia phase (line 220) for the as-received material. Thermodynamics of reactions of nickel phase reduction and oxidation was

analysed by calculating the changes in Gibb's free energy (ΔG) using standard data [20].

Results and discussion

Thermodynamics of the Reduction and Oxidation Stages

It is known [21] that in the temperature range 630–680 °C, a transition from diffusion to kinetic mechanism of oxidation occurs. Additionally, by analysing the thermodynamics of reduction and oxidation stages, it was revealed that in the temperature range 600–800°C, the change in Gibb's free energy (ΔG) is more negative and the equilibrium constant (K) is considerably higher for the reaction of nickel oxidation compared to its reduction (see Table 2).

Table 2. The data of thermodynamics of reduction and oxidation stages for the material tested

Reaction	Gibb's free energy (ΔG, kJ/mol) at 600°C	Equilibrium constant (K) at 600°C	Gibb's free energy (ΔG, kJ/mol) at 800°C	Equilibrium constant (K) at 800°C
Reduction	-41	$2.7 \cdot 10^2$	-43	$1.3 \cdot 10^2$
Oxidation	-159	$3 \cdot 10^9$	-145	$1 \cdot 10^7$

According to this, we concluded that during redox cycling at higher temperature, the Ni oxidation stage becomes more faster than the NiO reduction one. Thus, the probability of retaining unreduced particles is high, if the reduction period was too short. In such a case, the resulting structure does not meet the requirements on uniformity and, finally, efficiency of an anode substrate.

The Treatment Temperature of 600°C

Exposition of YSZ–NiO ceramics at the temperature 600°C for 4 h in the Ar–5 vol% H_2 mixture that can be used for gradual reduction of SOFC anodes (version 1 in Table 1) causes partial reduction of the NiO particles by a diffusion mechanism. Thin Ni edgings (of thickness of 0.1–0.3 μm) are formed around NiO particles (Fig. 3a).

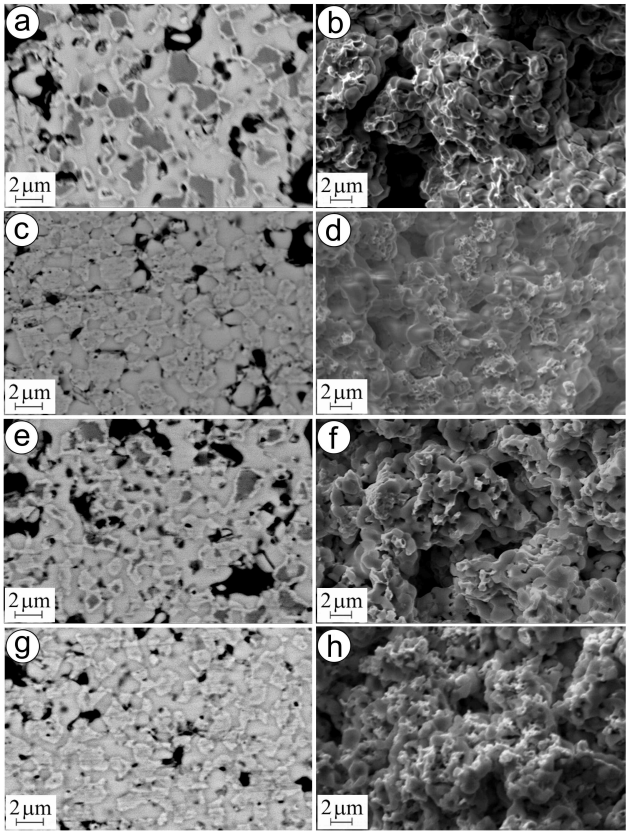

Figure 3. SEM microstructures (a, c, e, g – BSD images) and microfractographs (b, d, f, h – SE images) for the material in versions 1 (a, b), 2 (c, d), 3 (e, f) and 4 (g, h) (see Table 1).

The substructure of these edgings was evaluated using X-ray data on average size of coherent dispersion areas of nickel phase (D) (Fig. 4(a)). This parameter was measured as 45 nm. Reduction in strength to 84% of the value

for the asreceived YSZ–NiO ceramics (Fig. 4(c)) is possibly caused by partial structural transformation of nickel phase followed by a little volume decrease. It is displayed in the mixed fracture micromechanism (Fig. 3b). Although, no noticeable change of zirconia skeleton was found for this variant of the treatment.

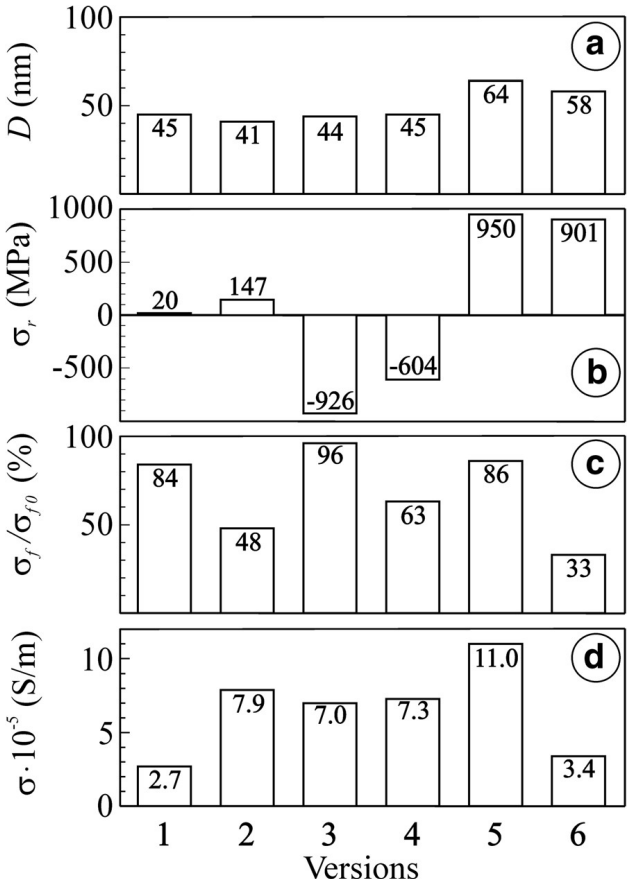

Figure 4. Average size of coherent dispersion area (*D*) (a), residual stresses (σ_r), in zirconia phase (b), relative strength (σ_f / σ_{f0}) (c) and specific electrical conductivity (σ) (d) for the material in versions 1–6 (see Table 1). The numbers on the bars indicate the values of corresponding parameters.

As compared to the as-received material, residual stresses did not change as well (Fig. 4(b)). The electrical conductivity of the material of $2.7 \cdot 10^5$ S/m is provided by thin films of Ni around NiO particles united into the network (Fig. 4(d)). More intensive reduction of YSZ–NiO ceramics by the same diffusion mechanism occurs in pure hydrogen (version 2 in Table 1). During 4 h, the structure of completely reduced Ni particles is formed (Fig. 3c). The substructure parameter (average size *D*) of these particles was measured as 41 nm that is less than for version 1 (Fig. 4(a)). Simultaneously, the volume decrease of initial NiO particles of 41.6% occurs [22]. Nanopores on Ni particles formed due to their shrinkage as well as the pores between the particles prevent the rise of residual tensile stresses (Fig. 4(b)).

Nickel phase transformation followed by volume change and formation of pores causes the loss of a significant percentage of particle bonds and violate material integrity which is displayed in the predominantly intergranular fracture micromechanism (Fig. 3d). Reduction in strength to 48% of the value for the as-received YSZ–NiO ceramics is recognized (Fig. 4(c)). Thanks to complete reduction of nickel phase, the high electrical conductivity (Fig. 4(d)) of the material is achieved compared to the similar functional materials [23]. According to our data [4], there exists a substantial difference in the mechanical behaviour of NiO ceramics after redox treatment as compared to that of the singly reduced material, at the treatment temperature of 600 °C. During the

treatment, structural transformation of boundaries of contacting nickel phase particles occurs, causing an increase in strength. The cleavage fracture micromechanism was noted in the specimens tested. This micromechanism corresponds to the higher cohesive strength of nickel phase particles as compared to the ultimate cleavage stress of the particles themselves. Such treatment technique has been used in this work for improvement of strength and electrical conductivity of YSZ–NiO ceramics. Upon redox cycling, exposition of the material at the temperature 600 °C for 4 h in air resulted in complete oxidation of preliminarily reduced Ni edgings on NiO particles (version 3 in Table 1, Fig. 3e) as well as of preliminarily reduced Ni particles (version 4, Fig. 3g) by diffusion mechanism. After five cycles of the redox treatment at 600 °C with final reduction stage (version 3), most of NiO particles were reduced completely, forming a continuous network of electrically conducting material in the zirconia skeleton (Fig. 3e) which resulted in the value of specific electrical conductivity of the material of $7 \cdot 10^5$ S/m (Fig. 4(d)). Fragmentation of coarse grains of nickel phase resulted in more fine structure of the material treated. The substructure parameter (D) of reduced particles for version 3 was measured as 44 nm which is similar to that for version 1 (Fig. 4(a)). Thus, no distinct change of substructure of nickel particles was found.

The X-ray data displayed a reduction of 2Θ angle for cyclically treated materials. In accordance with Wolf–Bragg's law

$$2d \sin\Theta = n\lambda \qquad (2)$$

where n is the positive integer and λ is the wavelength of incident wave; the spacing between the planes in the atomic lattice (d) of zirconia phase increases resulting (see Eq. (1)) in considerable relaxation of residual stresses (σ_r) in the material of versions 3 and 4 as compared to the as-received material (Fig. 4(b)). This affects positively the mechanical behaviour of the material, especially of version 3 (Fig. 4(c)). The mixed fracture micromechanism was noted in tested specimens of versions 3 (Fig. 3f) and 4 (Fig. 3h). The fracture surfaces comprise brittle cleavage areas of ceramic matrix neighbouring to ductile fracture ones of reduced nickel (Fig. 3f). Like for the NiO ceramics treated [4], this corresponds to higher cohesive strength between the particles of zirconia and nickel phase as compared to the singly reduced material.

The Treatment Temperature of 800°C

In order to reduce the redox treatment duration, the behaviour of YSZ–NiO ceramics was estimated under redox cycling at 800 °C. During single exposition of the material in the Ar–5 vol% H_2 mixture at this temperature (version 5 in Table 1), NiO particles are reduced completely within 1 h (Fig. 5a) by diffusion mechanism of much higher intensity as compared to version 1. Reduced Ni particles are

dotted with nanopores. The NiO to Ni transformation is carried out rapidly with formation of comparatively coarse substructure (parameter *D* of reduced particles was measured as 64 nm, see Fig. 4(a)). The X-ray data display the increase of the 2Θ angle for the material singly reduced at 800 °C. Consequently, the spacing between the planes in the atomic lattice (*d*) of the zirconia phase decreases, resulting in considerable growth of residual stresses (σ_r) in the material of version 5 as compared to the as-received material (Fig. 4(b)). The singly reduced material has somewhat lower strength as compared to as-received ceramics (Fig. 4(c), version 5) but substantially higher electrical conductivity as compared to the material treated at 600 °C (Fig. 4(d), versions 5 and 1, respectively).

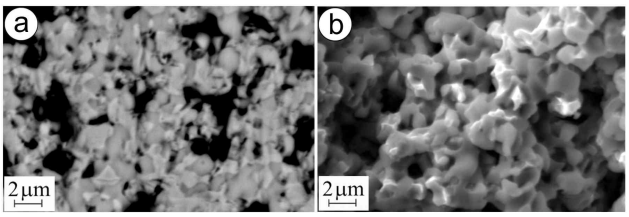

Figure 5. SEM microstructures (a – BSD image) and microfractograph (b – SE image) for the material in version 5 (see Table 1).

The mixed fracture micromechanism is recognized in the specimens tested (Fig. 5b). It is similar to the one after the redox treatment of YSZ–NiO ceramics at 600 °C. It also evidences that single reduction at 800 °C does not violate the integrity of the zirconia skeleton and a partial decrease in strength is caused by nickel phase transformation.

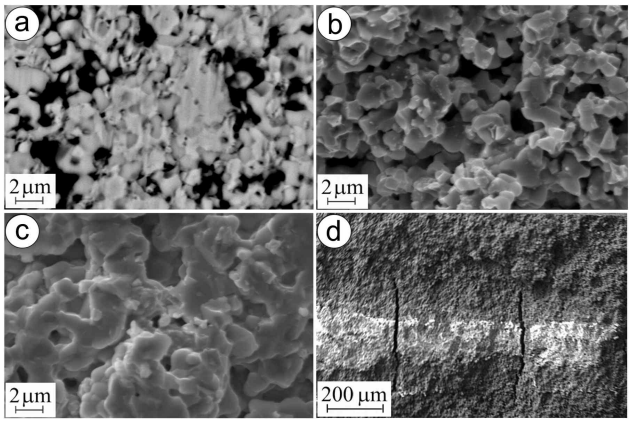

Figure 6. SEM microstructure (a – BSD image) and microfractographs (b-d – SE images) for the material in version 6 (see Table 1).

Contrary to the positive effect of redox treatment of YSZ–NiO ceramics at 600 °C, a negative tendency for strength of YSZ–NiO ceramics during the treatment at 800 °C is noted (Fig. 4(c), version 6). In both cases of the treatment of YSZ–NiO ceramics, the resulting structures are similar (Fig. 6a as compared to Fig. 3e) except for the peculiar (of green colour) inner part of specimens after the treatment at 800 °C (Fig. 6d).

As stated above, a kinetic mechanism of oxidation at this temperature intensifies the growth of unreduced volume of the anode during redox cycling. Two different areas on the fracture surface picture of a specimen treated at 800 °C are observed. In the reduced layer, mixed fracture micromechanism comprising transgranular cleavage of zirconia particles and intergranular fracture along the boundaries of contacting nickel phase particles dominates (Fig. 6b). The nickel particles of smaller sizes

had possibly agglomerated on zirconia particles. Being intact, they are separated by a network of the pores formed during the redox treatment. Thus, this fracture micromechanism is as energy expensive as the one revealed for the material after the redox treatment at 600 °C (Fig. 3f). In the unreduced inner layer of the anode transgranular cleavage, a fracture of coarse zirconia and nickel oxide agglomerates dominates, and occasionally, the signs of intergranular fracture along the boundaries of particles of smaller size are observed (Fig. 6c). In spite of similar levels of residual stresses in the zirconia phase that were estimated for the entire reduced volume (Fig. 4(b), version 5) and outer reduced layer (version 6), respectively, different structural factors affect the integrity of these materials. The total strength of the material after redox treatment at 800 °C is decreased considerably with the array of microcracks in the bulk of the specimen (Fig. 6d) that have formed during the treatment normally to its surface. These microcracks are nucleated following a stress gradient on the boundaries between reduced and unreduced layers as a result of thermal expansion (thermal expansion coefficients for YSZ, NiO and Ni phases are $10.9 \cdot 10^{-6}$, $14.1 \cdot 10^{-6}$ and $16.4 \cdot 10^{-6}$/K, respectively [24]). The reduced layer showed the value of specific electrical conductivity $3.4 \cdot 10^{5}$ S/m (Fig. 4(d), version 6) which is satisfactory for SOFC anodes. However, this value is lower than that of the material singly reduced at 800 °C (version 5). Besides, the unreduced layer having very low electrical conductivity becomes a substantial obstacle in achieving the required electrochemical performance of the fuel cell. Thus, contrary to the positive effect of redox treatment at 600 °C on strength and electrical conductivity of YSZ–NiO ceramics, such treatment at 800 °C causes the formation of anode structure with reduced outer and unreduced inner layers as well as the array of microcracks in the bulk of an anode initiated normally to its surface, what causes the loss of its integrity. The unreduced inner layer of the anode has unsatisfactory electrical conductivity.

Oxidation resistance of MAX-phases at 600 °C in air

The dependences of weight gain per unit surface area on oxidation time at 600 °C for Ti_3AlC_2 based materials tested are presented in Fig. 7. It can be seen that the $\Delta W/S$ for material with porosity of 22 % monotonically increases and reaches the value of 24 mg/cm^2 after exposition of 437 h. The rapid oxidation of this material can be explained by intense penetration of oxygen into material through the pores. As a result, not only outer surface of the specimen but also the surfaces of pores in the bulk material were oxidized (Fig. 8a, b).

The oxidation kinetics for Ti_3AlC_2 based material with 1 % porosity at 600 °C remarkable increases on the first stage of the test (Fig. 7). After 15 h the weight gain per unit surface area

increases more slowly and after 1000 h exposition is 1.0 mg/cm^2. Table 3 presents an average quantity of chemical elements in bulk material and a film, obtained by EDS method.

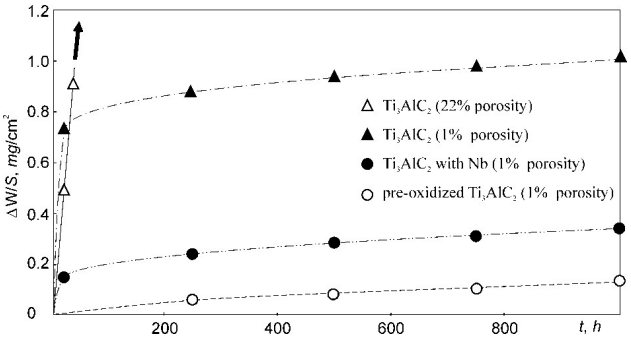

Figure 7. Oxidation kinetics for the MAX-phase at 600 °C in air

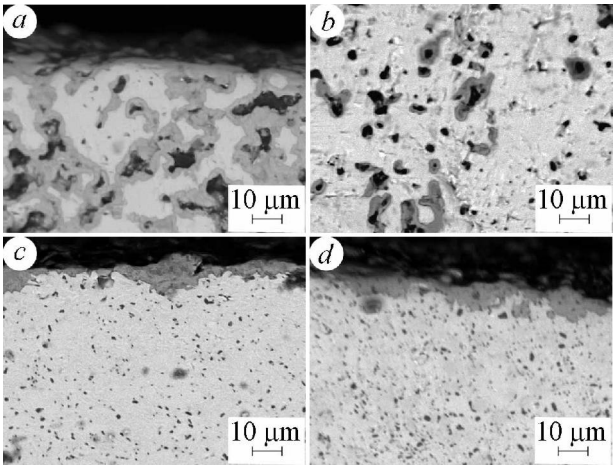

Figure 8. Back-scattered electron images of the films formed at 600 °C for 1000 h: (a) Ti_3AlC_2 based material with 22 % porosity; (b) oxidized pores of Ti_3AlC_2 based material with 22 % porosity; (c) Ti_3AlC_2 based material with 1 % porosity; (d) Nb doped Ti_3AlC_2 based material with 1 % porosity.

It can be seen that carbon is missed in the film while oxygen is presented in excessive amounts. This means that the surfaces of Ti_3AlC_2 and TiC particles are completely oxidized to TiO_2, Al_2O_3 and gaseous CO or CO_2 phase which volatilizes from the film. The overall equations for the oxidation reactions is,

$$4Ti_3AlC_2 + 23O_2 = 12TiO_2 + 2Al_2O_3 + 8CO_2\ (g),$$

$$TiC + 2O_2 = TiO_2 + CO_2\ (g).$$

Table 3. EDS analysis results of the Ti_3AlC_2 based materials with 1 % porosity (at. %)

Materials	Ti		Al		C		Nb		O	
	B	F	B	F	B	F	B	F	B	F
Ti_3AlC_2	51.3	23.7	14.8	8.1	34.6	0	0	0	0	68.2
Ti_3AlC_2 with Nb	44.1	25.3	14.9	3.3	42.8	0	1.4	0.6	0	70.1

B – bulk material, F - film

Wang and Zhou [14] had demonstrated that the film formed at 600 °C on the surface of Ti_3AlC_2 material with 5 vol. % TiC consisted of amorphous Al_2O_3, anatase and rutile TiO_2. The formation of anatase from Ti_3AlC_2 led to increase of stress due to the difference of their volume expansion coefficients. Therefore, the rapid increase of ΔW/S value for Ti_3AlC_2 based material with 1 % porosity on the first stage of the test can be associated with intense film formation as well as with low protective ability property of the thin film due to microcracks, and also with penetration of oxygen through micropores into bulk material. After long-term exposition, when micropores were covered with oxides and the film thickness was increased (Fig. 8c), the inward diffusion of oxygen and outward diffusion of Ti and Al became slowly. As a result the oxidation kinetics was decreased. Based on these results it can be assumed that the preliminary oxidation to form the protective

layer of oxides would improve the oxidation resistance of Ti_3AlC_2 based materials. The pre-oxidation at 1000–1300 °C for 2 h provides the formation of a dense film which consists of Al_2O_3 and rutile TiO_2 without anatase TiO_2 [25]. In present study the pre-oxidation of Ti_3AlC_2 based material with 1 % porosity was performed at 1200 °C in air for 2 h. The long-term oxidation resistance was investigated at 600 °C in air for 1000 h. As can be seen from Fig. 7 the pre-oxidized material does not demonstrate any discernible increase of weight gain per unit surface area during whole the test. The value of ΔW/S for this material does not exceed 0.11 mg/cm^2 after 1000 h exposition.

The influence of Nb on the oxidation resistance of Ti_3AlC_2 based material with 1 % porosity had been investigated. Despite a greater content of TiC, the weight gain per unit surface area for this material increases more slowly as compared to material without Nb (Fig. 7). The ΔW/S is 0.34 mg/cm^2 after exposition for 1000 h at 600 °C. This value is approximately 3 times smaller than that for Ti_3AlC_2 based material without Nb. Barsoum et al. [26] had shown that TiC has a deleterious effect on the oxidation kinetics of Ti_3SiC_2 based materials which also belong to the isotypic structure $M_{n+1}AX_n$. The contradiction of this conclusion with the results obtained in the present work can be explained by positive effect of Nb on the oxidation resistance of Ti_3AlC_2 based material. The EDS analysis shows that the content of Ti, Al and Nb in the film of Ti_3AlC_2 based material with Nb is less than that in the bulk material (Table 3). On the other hand, the content of Al in the film of this material is significantly less than that of material without Nb. Therefore, it is reasonable to assume that the film of Ti_3AlC_2 based material with Nb consists mainly of TiO_2 and of minor quantity of Al_2O_3 (Fig. 8d). According to [12], the formation of dense Al_2O_3 layer is responsible for high oxidation resistance of Ti_3AlC_2 based materials. Thus, the material with Nb ought to be less oxidation resistant than material without Nb. Jiang et al. [27] had concluded that Nb in solid solution with TiO_2 improves the oxidation resistance of Ti–Al–Nb alloys by impeding mass transformation in TiO_2. Evidently in case of Ti_3AlC_2 based materials the positive effect of Nb manifests in the same manner.

Conclusions

A cyclic treatment technique (redox cycling) comprising stages of material exposition in reducing and oxidizing high-temperature gas environments and intermediate degassing between these stages has been developed to improve the strength and electrical conductivity of YSZ–NiO ceramic anode substrates for solid oxide fuel cells. Based on the experimental data, we suppose that redox cycling at 600 °C is the most ideal for this material. The parameters of the treatment (reduction dwell time not less than 4 h under the pressure of the Ar–5 vol% H2 mixture of 0.15

MPa; oxidation dwell time 4 h) allow a structure to be formed which provides improved physical and mechanical properties of the material. In such a structure, according to the X-ray analysis, a substantial drop of residual stresses is achieved as compared to the one-time reduced material.

The oxidation resistance of MAX-phase based materials had been studied at 600 °C in static air for 1000 h. The results showed that the weight gain per unit surface area for sintered Ti_3AlC_2 based material with porosity of 22 % increased gradually and after 437 h reached the value of 24 mg/cm^2. The drastic increase of oxidation kinetics of this material was caused by intense oxidation not only the outer surface of specimen but also the surfaces of pores. The weight gain per unit surface area for hot pressed Ti_3AlC_2 based material with 1 % porosity intensively increased for the first 15 h of oxidation and then the oxidation kinetics slowly decreased. The pre-oxidation at 1200 °C for 2 h eliminated the initial oxidation of this material at 600 °C. It was revealed that the additional doping with Nb significantly improves the oxidation resistance of Ti_3AlC_2 based material.

References

[1] Sarantaridis D, Atkinson A. Redox cycling of Ni-based solid oxide fuel cell anodes: a review. Fuel Cells 2007; 3:246-258

[2] Ettler M, Timmermann H, Malzbender J et al. Durability of Ni anodes during reoxidation cycles. J. Power Sources 2010; 195:5452-5467

[3] Wood A, Waldbillig D. Preconditioning treatment to enhance redox tolerance of solid oxide fuel cells. United States patent 20118029946 B2. 2011 Oct 4.

[4] Podhurs'ka VY, Vasyliv BD, Ostash OP et al. Structural transformations in the NiO-containing anode of ceramic fuel cells in the course of its reduction and oxidation. Materials Sci 2014; 49(6):805-811

[5] Ostash OP, Vasyliv BD, Podhurs'ka VY et al. Optimization of the properties of 10Sc1CeSZ–NiO composite by the redox treatment. Materials Sci 2011; 46(5):653-658

[6] Vasyliv BD, Podhurs'ka VY, Ostash OP et al. Influence of reducing and oxidizing media on the physicomechanical properties of ScCeSZ–NiO and YSZ–NiO ceramics. Materials Sci 2013; 49(2):135-144

[7] Radovic M, Barsoum MW (2013) MAX phases: bridging the gap between metals and ceramics. Amer Ceram Soc Bull 92(3):20–27

[8] Barsoum MW, Yoo H-I, Polushina IK et al. (2000) Electrical conductivity, thermopower, and Hall effect of Ti_3AlC_2, Ti_4AlN_3, and Ti_3SiC_2. Phys Rev 62(15):1094–1098

[9] Prikhna T, Cabioc'h T, Gawalek W et al. (2014) Study of thermal stability and mechanical characteristics of MAX-phases of Ti–Al–C(N) system and their solid solutions. Advan Sci Technol 89:123–128

[10] Barsoum MW, Tzenov N, Procopio A et al. (2001) Oxidation of $Ti_{n+1}AlX_n$ (n = 1-3 and X = C, N): II. Experimental Results. J Electrochem Soc 148(8):551–562. doi:10.1149/1.1380256

[11] Song GM, Pei YT, Sloof WG et al. (2008) Early stages of oxidation of Ti_3AlC_2 ceramics. Mater Chem Phys 112:762–768

[12] Wang XH, Zhou YC (2003) Oxidation behavior of Ti_3AlC_2 at 1000–1400 °C in air. Corros Sci 45:891–907

[13] Taotao A (2012) High-temperature oxidation behavior of un-dense Ti_3AlC_2 material at 1000 °C in air. Ceram Int 38:2537–2541

[14] Wang XH, Zhou YC (2003) Oxidation behavior of TiC-containing Ti_3AlC_2 based material at 500–900 °C in air. Mat Res Innovat 7:381–390. doi:10.1007/s10019-003-0278-7

[15] Pang WK, Low IM, O'Connor BH et al (2009) Oxidation characteristics of Ti_3AlC_2 over the temperature range 500–900 °C. Mater Chem Phys 117:384–389

[16] Podhurska V, Vasyliv B. Influence of redox treatment temperature on microstructure and properties of Ni-ZrO_2 anode materials. Proceedings of the International Conference on Oxide Materials for Electronic Engineering (OMEE-2014); 2014, May 26-30; Lviv, Ukraine. Lviv, Publishing House of Lviv Polytechnic; 2014.

[17] Tikekar N, Armstrong T, Virkar A. Reduction and reoxidation kinetics of Ni-based SOFC anodes. J. Electrochem. Soc 2006; 153:A654-A663

[18] Akselrud LG, Zavalii PY, Grin YN et al (1993) Use of the CSD program package for structure determination from powder data. Mat Sci Forum 133:335-342. doi:10.4028/www.scientific.net/MSF.133-136.335

[19] Sun B, Rudkin RA, Atkinson A. Effect of thermal cycling on residual stress and curvature of anode-supported SOFCs. Fuel Cells 2009; 6:805-813

[20] Mills I, Cvitas T, Homann K et al. Quantities, units and symbols in physical chemistry. Oxford: BLACKWELL SCIENCE LTD.; 1993, pp.1-165.

[21] Peraldi R, Monceau D, Pieraggi B. Correlations between growth kinetics and microstructure for scales formed by high-temperature oxidation of pure nickel. I. Morphologies and microstructures. Oxid. Met 2002; 58:249-273

[22] Faes A, Nakajo A, Hessler-Wyser A et al. Redox study of anode-supported solid oxide fuel cell. J. Power Sources 2009; 193:55-64

[23] Zhang Y, Liu B, Tu B et al. Redox cycling of Ni–YSZ anode investigated by TRP technique. Solid State Ion 2005; 176:2193-2199

[24] Mori M, Yamamoto T, Itoh H et al. Thermal expansion of nickel-zirconia anodes in solid oxide fuel cells during fabrication and operation. J. Electrochem. Soc 1998; 145:1374-1381

[25] Wang XH, Zhou YC (2003) Improvement of intermediate-temperature oxidation resistance of Ti_3AlC_2 by pre-oxiadtion at high temperatures. Mat Res Innovat 7:205–211. doi:10.1007/s10019-033-0252-4

[26] Barsoum MW, El-Raghy T, Ogbuji LUJT (1997) Oxidation of Ti_3SiC_2 in air. J Electrochem Soc 144:2508–2516. doi: 10.1149/1.1837846

[27] Jiang H, Hirohasi M, Lu Y et al. (2002) Effect of Nb on the high temperature oxidation of Ti–(0–50 at. %)Al. Scripta Mater 46:639–643